Electronic Supplementary Information

High Sensitivity Luminescent Sensor for Cortisol of Stress Biomarker by Four-Fold Interpenetrated Europium-Organic Frameworks Integrated with Logic Gate

Meng-Hua Tang, Ying Shi, Xiao-Lei Jiang, Hang Xu*, Yue Ma, and Bin Zhao*

Department of Chemistry, Key Laboratory of Advanced Energy Material Chemistry, MOE Nankai University, Tianjin 300071, China

*E-mail: xuhang@mail.nankai.edu.cn; zhaobin@nankai.edu.cn

X-Ray crystallography

Suitable crystals **MHT-1** was paced in a cooled N_2 gas stream at ~120 K for crystallographic data collection on a SuperNova Single Crystal Diffractometer equipped with graphite-monochromatic Mo-Kα radiation (λ = 0.71073 Å). Data reduction included absorption was performed by using the SAINT program.The structures were solved by direct methods and refined by full-matrix least squares on F^2 with SHELXS-97 and SHELXL-97 programs.All the hydrogen atoms were placed geometrically and refined using a riding model.

We used PLATON/SQUEEZE to calculate the contribution to the diffraction from the solvent region. The number of isolated H_2O and DMA molecules was determined by TG analyses and elemental microanalyses. Detailed crystal data and structure refinement for **MHT-1** was shown in **Table S1**.

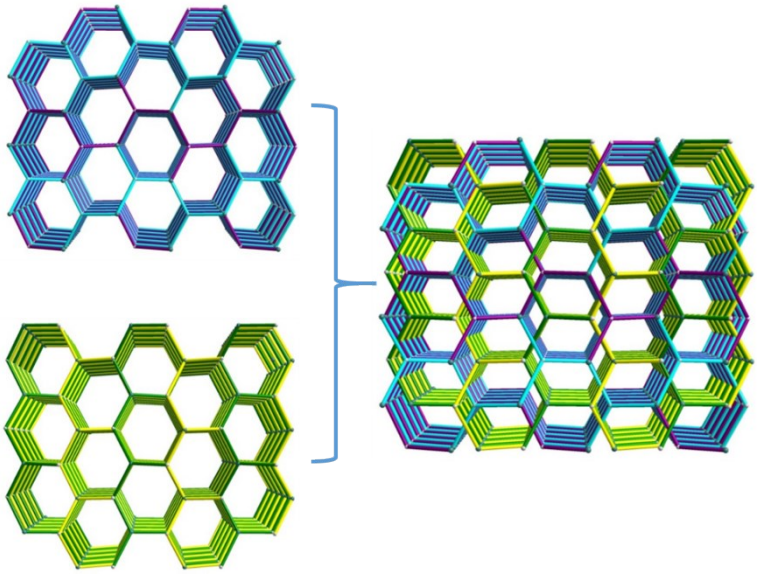

Fig. S1. The simplified topology of **MHT-1** with a [2+2] mode.

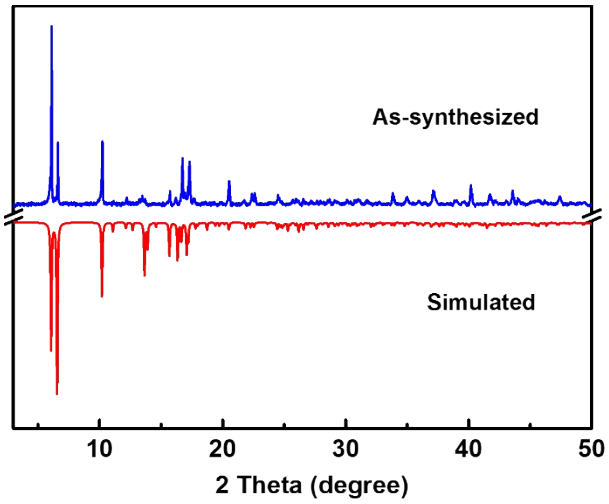

Fig. S2. The PXRD patterns of as-synthesized **MHT-1** and simulated one based on single-crystal data.

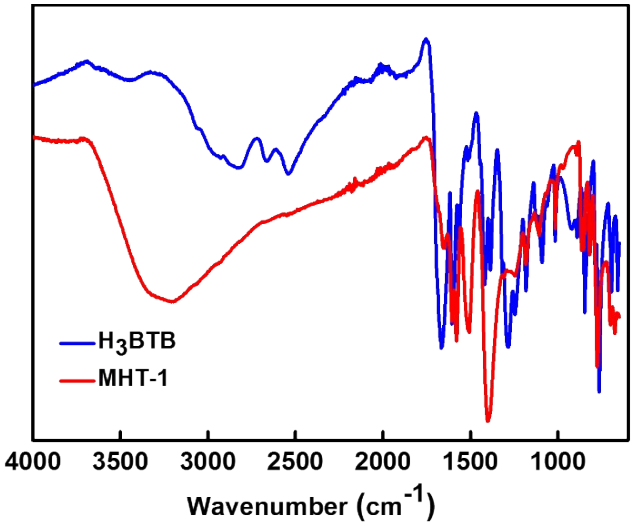

Fig. S3. The FT-IR spectra of H_3BTB ligand and **MHT-1**.

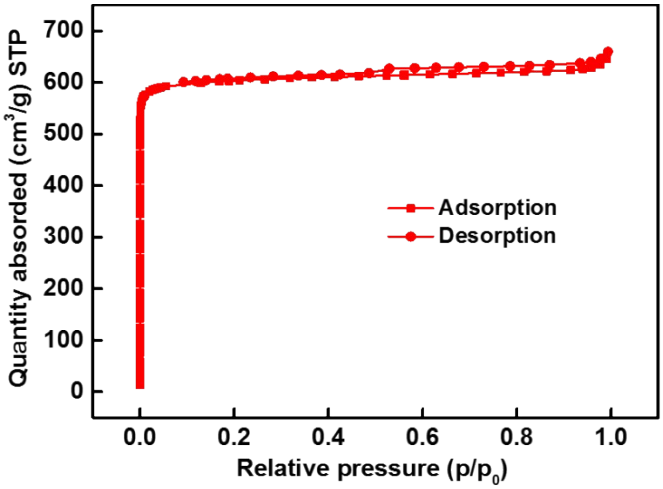

Fig. S4. N_2 adsorption-desorption isotherm of **MHT-1**.

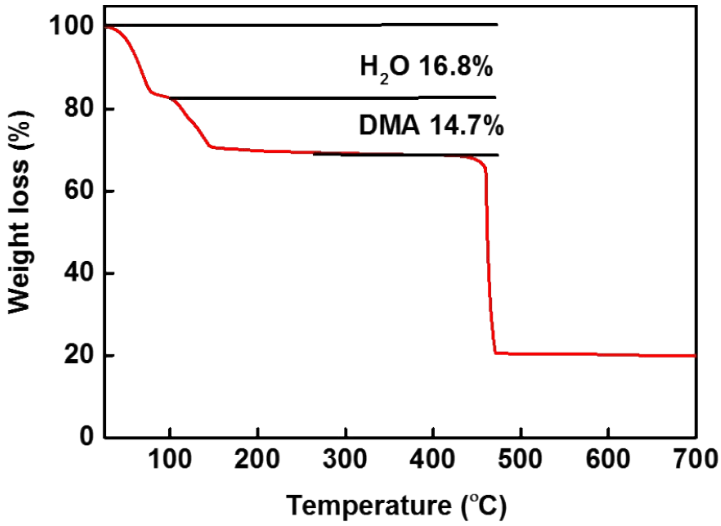

Fig. S5. TGA curve of **MHT-1**.

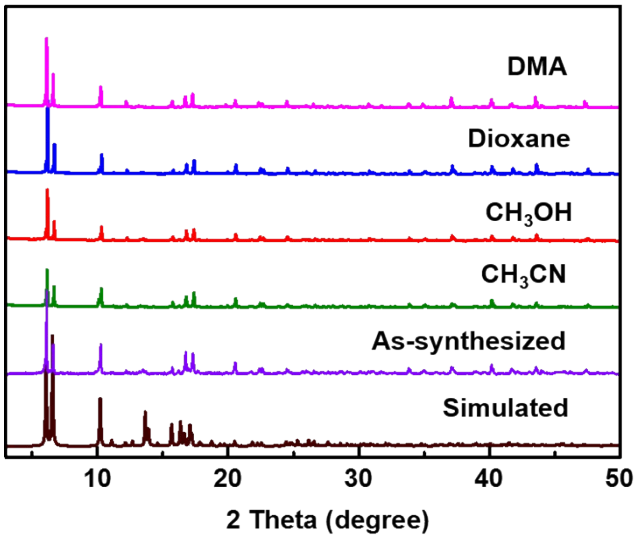

Fig. S6. The PXRD patterns of **MHT-1** after immersing in common organic solvents.

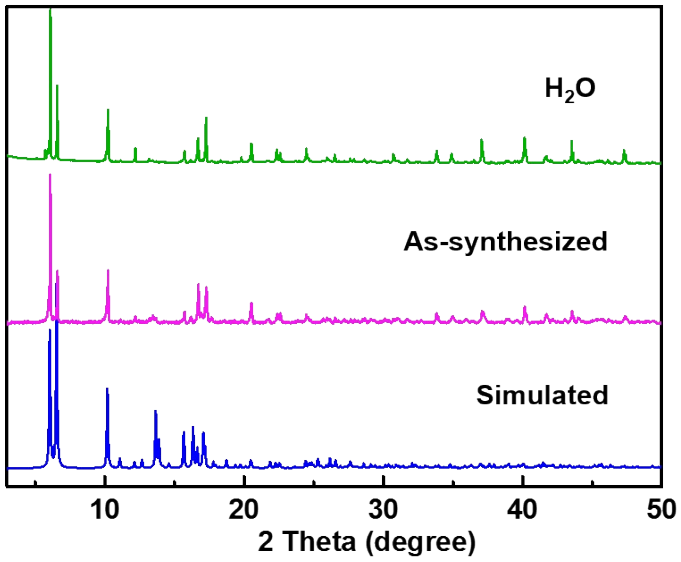

Fig. S7. The PXRD patterns of **MHT-1** after soaking in water for 12 h.

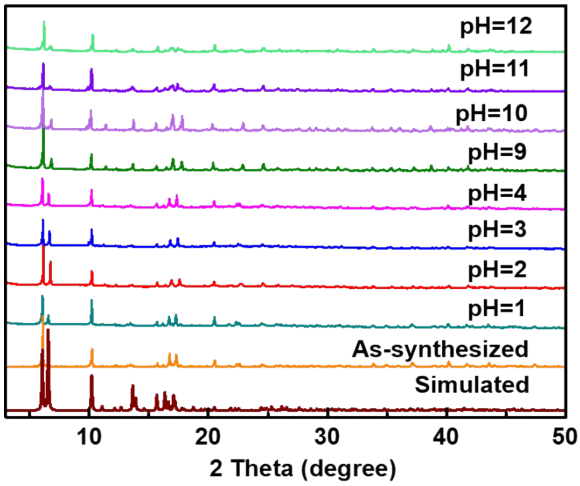

Fig. S8. The PXRD patterns of **MHT-1** treated by aqueous solutions with pH ranging from 1 to 12.

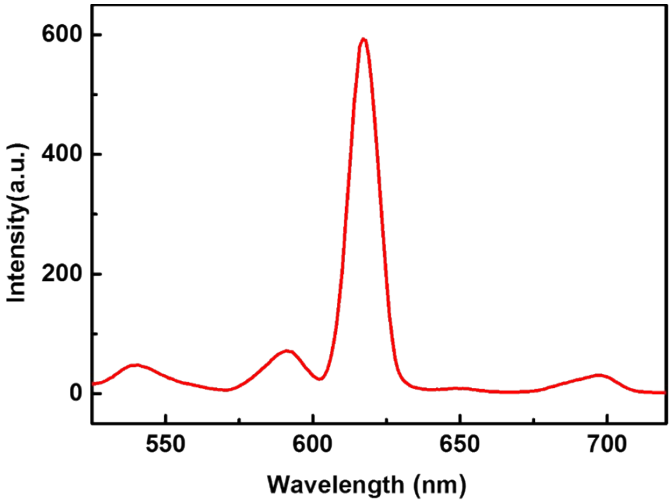

Fig. S9. The luminescence emission spectrum of **MHT-1**.

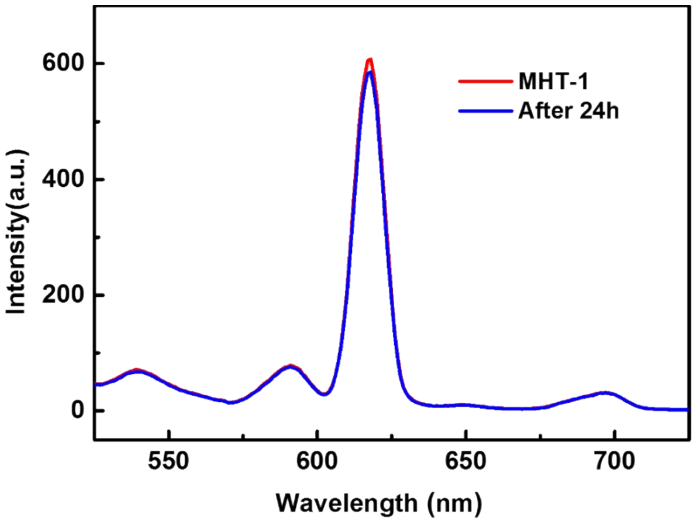

Fig. S10. Luminescence spectra of **MHT-1** original and after immersed in water for 24 hours.

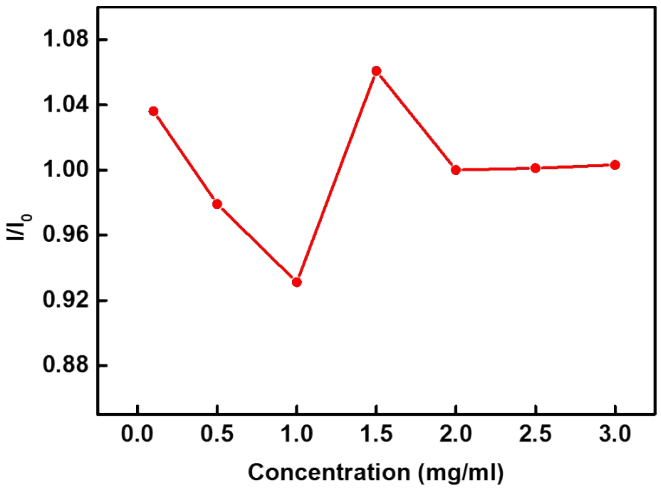

Fig. S11. The relationship between relative luminescent intensity of **MHT-1** and cortisol concentration.

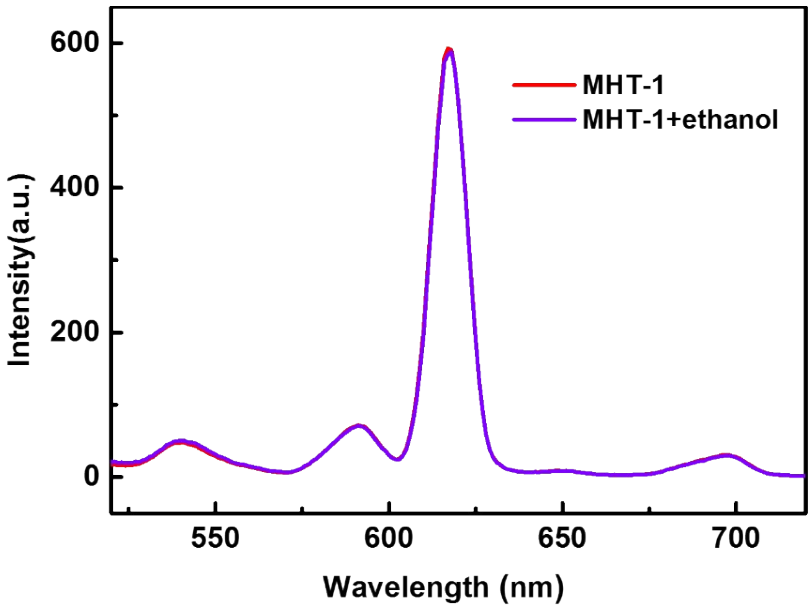

Fig. S12. Luminescence spectra of **MHT-1** and when ethanol was added.

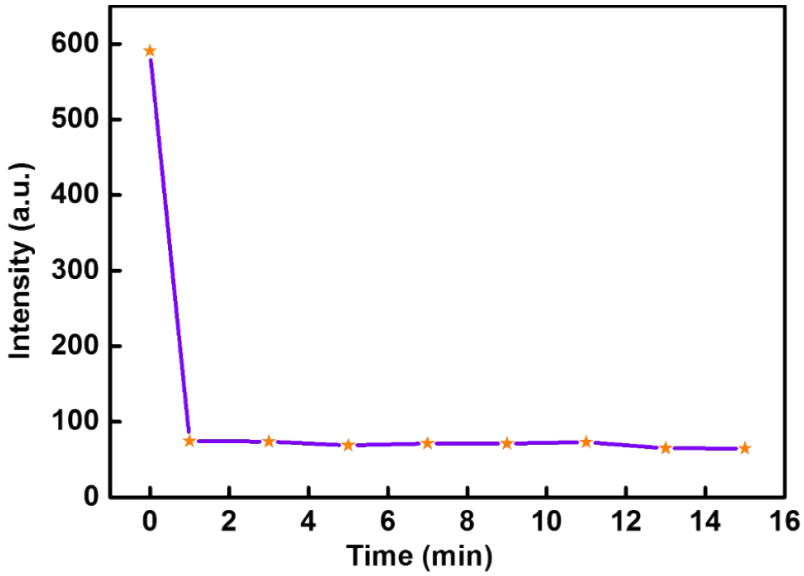

Fig. S13. Time-dependent luminescence intensity of **MHT-1** after the addition of cortisol.

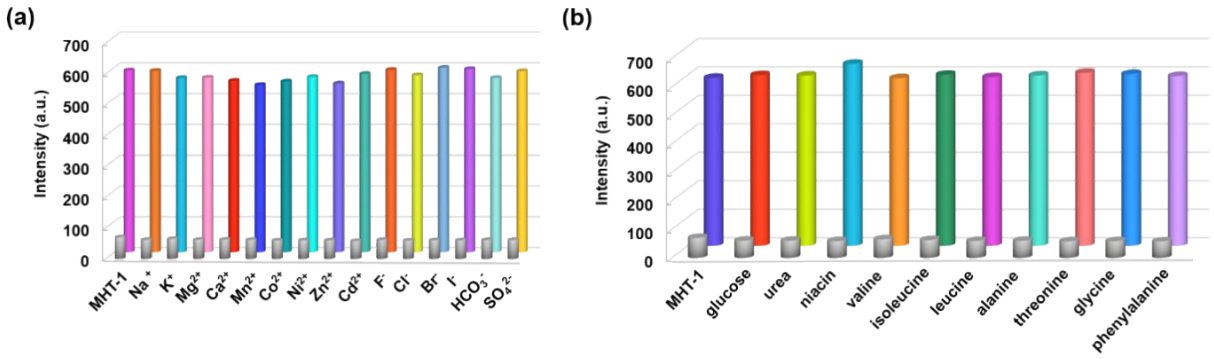

Fig. S14. Changes of luminescence intensity at 617 nm when cortisol was added into **MHT-1** solutions in the presence of (a) organic molecules, amino acids and (b) various kinds of cations and anions.

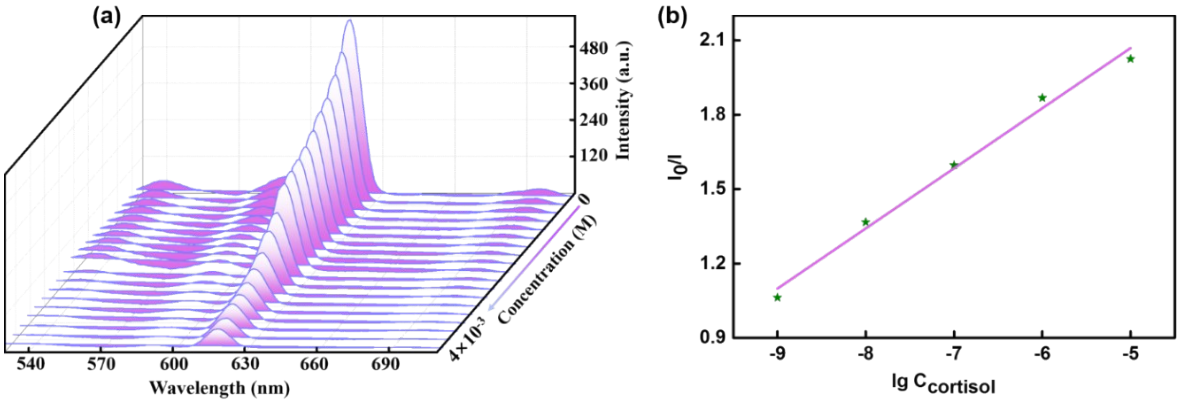

Fig. S15. (a) Luminescent response of **MHT-1** to cortisol in artificial sweat with cortisol concentration ranging from 10^{-9} M to 4×10^{-3} M. (b) Linear fitting in the low concentration range.

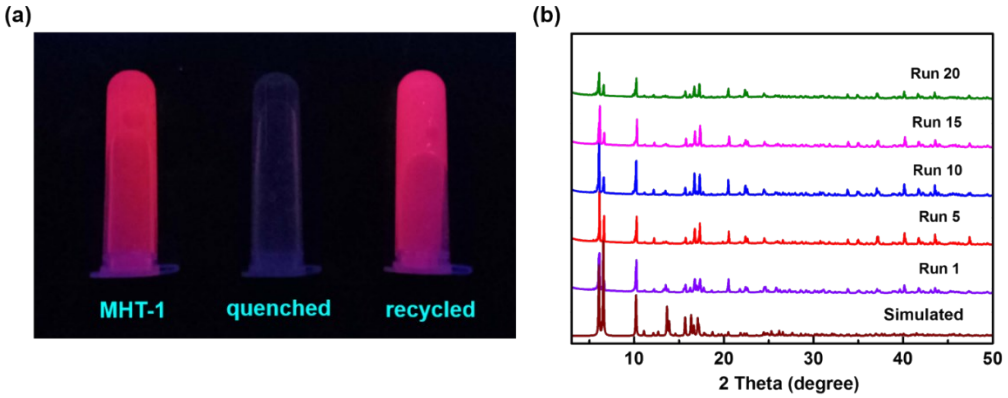

Fig. S16. (a) The luminescence change of **MHT-1** after quenching and recycling (irradiated by a 254 nm UV lamp). (b) PXRD of **MHT-1** after detecting cortisol 20 times.

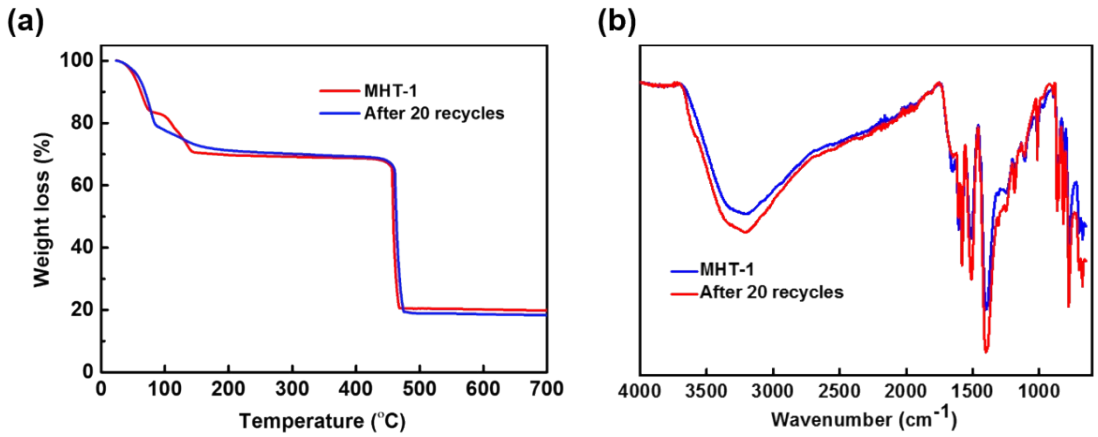

Fig. S17. (a) Thermogravimetric analyses of **MHT-1** and after 20 recycles, respectively. (b) The comparison of infrared spectroscopy between **MHT-1** and after

20 recycles of cortisol detection.

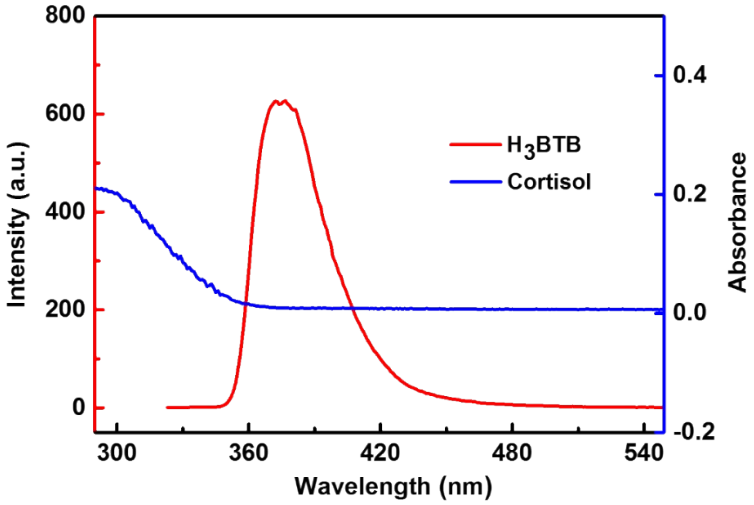

Fig. S18. Luminescence emission spectrum of H_3BTB and UV-Vis absorption of cortisol, respectively.

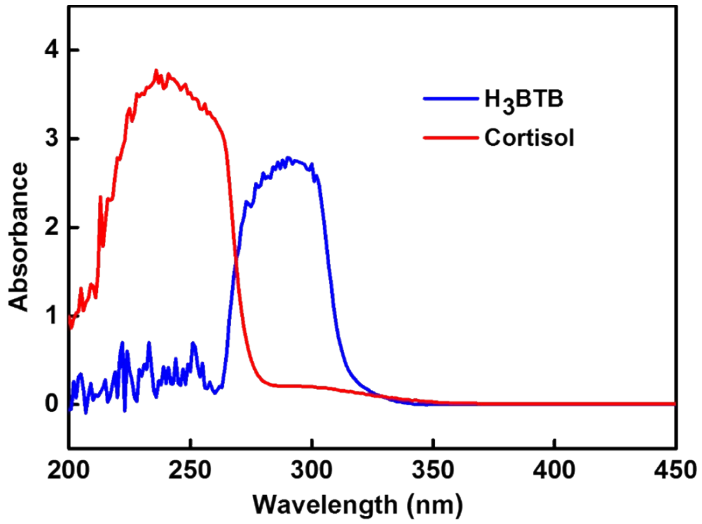

Fig. S19. UV-Vis spectra of cortisol and H_3BTB.

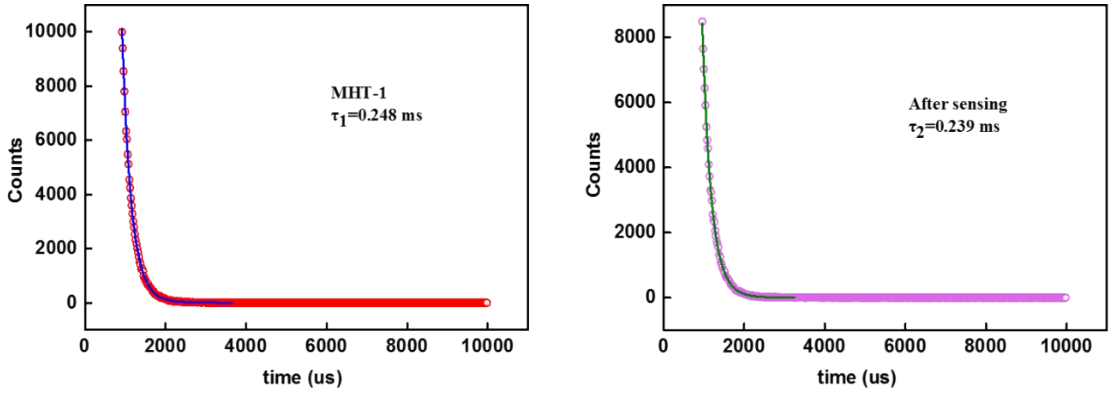

Fig. S20. Luminescence lifetime of **MHT-1** before and after sensing cortisol.

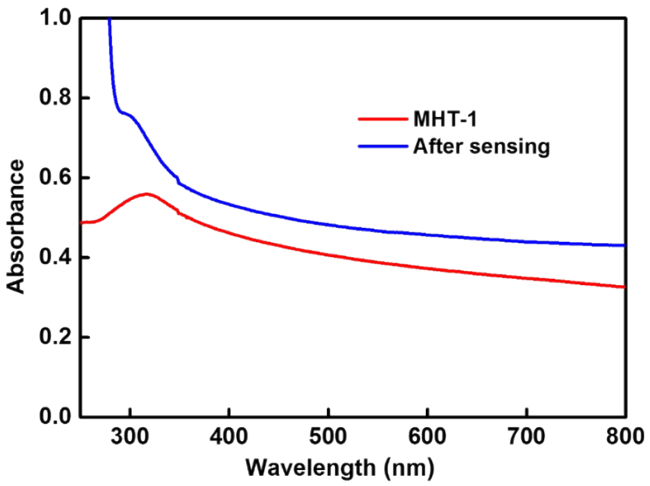

Fig. S21. Change of UV-Vis absorption of **MHT-1** after the addition of cortisol.

Table S1. Crystal data and structure refinement for **MHT-1**.

Identification code	**MHT-1**
Formula sum	$C_{33}H_{44.5}EuN_{1.5}O_{15.5}$
Formula weight	862.18
Temperature/K	123 (2)
Crystal system	orthorhombic
Space group	Pbca
a/Å	26.9686(10)
b/Å	7.3840(4)
c/Å	34.6549(13)
α/°	90
β/°	90
γ/°	90
Volume/Å3	6901.0(5)
Z	8
F(000)	3520.0
Goodness-of-fit on F2	1.067
Final R indexes [I>=2σ (I)]	R_1 = 0.0531, wR_2 = 0.1050
Final R indexes [all data]	R_1 = 0.0672, wR_2 = 0.1100

Table S2. List of Ln-MOFs with interpenetrated structures.

Compounds	Interpenetration	Reference
$(Me_2NH_2)[Ln(HL^1)_2(H_2O)_2]\cdot 1.5H_2O\cdot DMF$ (Ln = Ce, Pr, Nd, Sm)	8	1
MHT-1	**4**	**This work**
$[Ce_4(BINDI)_2(DMA)_{16}]\cdot[SiW_{12}O_{40}]\cdot 3DMA$	4	2
$[Ln(HL^2)(DMA)_2]\cdot DMA\cdot 2H_2O$ (Ln = La, Ce, Pr, Nd, Sm, Eu, Gd, Tb, Dy, Er)	3	3
Gd-pDBI	3	4
$\{(Me_2NH_2)[Tb(OBA)_2]\cdot(Hatz)\cdot(H_2O)_{1.5}\}_n$	3	5
$Tb_2(ADB)_3[(CH_3)_2SO]_4\cdot 16[(CH_3)_2SO]$	2	6
$[Eu(OH)(mip)]_n$	2	7
$[Me_2NH_2]_{24}[Tb_{12}(TATB)_{16}(HCOO)_{12}]\cdot 12DMF\cdot 48H_2O$	2	8
Ln-IAM-4	2	9
$Ln(BDC)_{1.5}(DMF)(H_2O)$ (Ln = Er, Tm)	2	10

H_3L^1 = tris((4-carboxyl)phenylduryl)amine, BINDI = N,N′-bis(5-isophthalate)-1,4,5,8-naphthalenediimide, DMA = N,N-dimethylacetamide, H_4L^2 = 5,5′-(2,3,5,6-tetramethyl-1,4-phenylene)bis(methylene)bis(azanediyl)diisophthalic acid, pDBI = (1,4-bis(5-carboxy-1H-benzimidazole-2-yl)benzene, OBA = 4,4′-oxybis(benzoate), Hatz = 3-amino-1,2,4-triazole, ADB = 4,4′-azodibenzoate, mip = 5-methylisophthalate ion, H_3TATB = 4,4’,4’’-s-triazine-2,4,6-tribenzoic acid, IAM = Institute of Advanced Materials, H_2BDC = 1,4-benzenedicarboxylic acid.

Table S3. A comparison of sensing rang and limit of detection (LOD) of cortisol in sweat with other reported methods.

	Method used	Concentration range	LOD	Reference
-	HPLC-MS/MS	0.1-25 ng/ml	0.04 ng/ml	11
nanoporous polyamide	ELISA	1-100 ng/ml	1 ng/ml	12
monooxygenase	FIA	0.98-10 µg/ml	0.98 µg/ml	13
aptamer	LFA	10-100 ng/ml	1 ng/ml	14
UV-LED	UV spectroscopy	0.5-5 µg/ml	0.2 µg/mL	15
TMB(Red)	CE-EIA-ED	0-60 ng/ml	0.6 ng/ml	16
β-MnO_2 CNs	EIS	0.03-54 pg/ml	0.008 pg/ml	17
MoS_2 nanosheets	EIS	1-500 ng/ml	1 ng/ml	18
e-RGO	ED	0.1-200 ng/ml	0.1 ng/ml	19
MIPs	ED	10-66 ng/ml	2.0 ng/ml	20
LTCC	ED	0.04-36 ng/ml	0.01 ng/ml	21
RTILs	ED	0.1-200ng/ml	0.1 ng/mL	22
FET	ED	10 fg/ml-10 ng/ml	1 pg/ml	23
ZnONRs/CCY	ED	1 fg/ml-1 µg/ml	0.098 fg/ml	24
EDL	ED	10-200 ng/ml	1 ng/ml	25
MHT-1	**LD**	**0.36 ng/ml-1450 µg/ml**	**0.36 ng/ml**	**This work**

ELISA = enzyme-linked immunosorbent assay, FIA = fluorimetric assay, LFA = lateral flow assay, UV-LED = UV light emitting diode, CE-EIA-ED = capillary electrophoretic enzyme immunoassay with electrochemical detection, e-RGO = electroreduced graphene oxide, EIS = electrochemical impedance spectroscopy, ED = electrochemical detection, MIPs = molecular imprinted polymers, LTCC = low temperature co-fired ceramic, RTILs = room temperature ionic liquids, FET = field-

effecttransistor, ZnONRs/CCY = ZnO nanorods - coated flexible carbon yarns, EDL = electrical double layer, LD = luminescent detection.

Table S4. The truth table of Gate 1, Gate 2 and Gate 3.

Gate 1	**Input 1A**		**Output 1**
	C > 8 ng/ml		Light 1
	0		1
	1		0
Gate 2	**Input 2**		**Output 2**
	Output 1	Input 1B (C > 140 ng/ml)	Light 2
	0	1	0
	0	0	1
Gate3	**Input 3**		**Output 3**
	Output 2		Light 3
	0		1
	1		0

References

1 Y. P. He, Y. X. Tan and J. Zhang, *Inorg. Chem.*, 2013, **52**, 12758–12762.

2 H. L. Zhang, J. Z. Liao, W. Yang, X. Y. Wu and C. Z. Lu, *Dalt. Trans.*, 2017, **46**, 4898–4901.

3 C. Wang, L. Li, J. G. Bell, X. Lv, S. Tang, X. Zhao and K. M. Thomas, *Chem. Mater.*, 2015, **27**, 1502–1516.

4 T. Kundu, S. Mitra, P. Patra, A. Goswami, D. Díazdíaz and R. Banerjee, *Chem. - A Eur. J.*, 2014, **20**, 10514–10518.

5 D. M. Chen, N. N. Zhang, C. S. Liu and M. Du, *J. Mater. Chem. C*, 2017, **5**, 2311–2317.

6 T. M. Reineke, M. Eddaoudi, D. Moler, M. O'Keeffe and O. M. Yaghi, *J. Am. Chem. Soc.*, 2000, **122**, 4843–4844.

7 Q. B. Bo, H. T. Zhang, H. Y. Wang, J. L. Miao and Z. W. Zhang, *Chem. - A Eur. J.*, 2014, **20**, 3712–3723.

8 Y. H. Han, C. B. Tian, P. Lin and S. W. Du, *J. Mater. Chem. A*, 2015, **3**, 24525–24531.

9 Z. Duan, Y. Li, X. Xiao, X. Huang, X. Li, Y. Li, C. Zhang, H. Zhang, L. Li, Z. Lin, Y. Zhao and W. Huang, *ACS Appl. Mater. Interfaces*, 2020, **12**, 18715–18722.

10 H. He, D. Yuan, H. Ma, D. Sun, G. Zhang and H. C. Zhou, *Inorg. Chem.*, 2010, **49**, 7605–7607.

11 M. Jia, W. M. Chew, Y. Feinstein, P. Skeath and E. M. Sternberg, *Analyst*, 2016, **141**, 2053–2060.

12 S. Upasham and S. Prasad, *Lab Chip*, 2020, **20**, 1947–1960.

13 D. Appel, R. D. Schmid, C. A. Dragan, M. Bureik and V. B. Urlacher, *Anal. Bioanal. Chem.*, 2005, **383**, 182–186.

14 S. Dalirirad and A. J. Steckl, *Sensors Actuators, B Chem.*, 2019, **283**, 79–86.

15 P. Ray and A. J. Steckl, *ACS Sensors*, 2019, **4**, 1346–1357.

16 M. Jia, Z. He, W. Jin, *J. Chromatogr. A*, 2002, **966**, 187–194.

17 Q. Zhou, P. Kannan, B. Natarajan, T. Maiyalagan, P. Subramanian, Z. Jiang, S. Mao, *Sensors Actuators, B Chem.*, 2020, **317**, 128134.

18 D. Kinnamon, R. Ghanta, K. C. Lin, S. Muthukumar, S. Prasad, *Sci. Rep.*, 2017, **7**, 1–13.

19 S. K. Tuteja, C. Ormsby, S. Neethirajan, *Nano-Micro Lett.*, 2018, **10**, 1–10.

20 S. M. Mugo and J. Alberkant, *Anal. Bioanal. Chem.*, 2020, **412**, 1825–1833.

21 A. Vasudev, A. Kaushik, Y. Tomizawa, N. Norena and S. Bhansali, *Sensors Actuators, B Chem.*, 2013, **182**, 139–146.

22 B. Jagannath, S. Muthukumar, S. Prasad, *Anal. Chim. Acta*, 2018, **1016**, 29–39.

23 H. J. Jang, T. Lee, J. Song, L. Russell, H. Li, J. Dailey, P. C. Searson and H. E. Katz, *ACS Appl. Mater. Interfaces*, 2018, **10**, 16233–16237.

24 S. Madhu, A. J. Anthuuvan, S. Ramasamy, P. Manickam, S. Bhansali, P.

Nagamony and V. Chinnuswamy, *ACS Appl. Electron. Mater.*, 2020, **2**, 499–509.

25 R. D. Munje, S. Muthukumar, A. Panneer Selvam and S. Prasad, *Sci. Rep.*, 2015, **5**, 1–11.